

Supporting information for;

P(V) Dications: Carbon-based Lewis acid initiators for Hydrodefluorination

Alexander E. Waked, Saurabh S. Chitnis, and Douglas W. Stephan*

Department of Chemistry, University of Toronto, 80 St. George St., Toronto, Ontario, M5S 3H6, Canada, Email: dstephan@chem.utoronto.ca

Table of Contents

1. General Considerations.....	3
2. Synthesis of P(V) Compounds.....	4
2.1 Synthesis of [(terpy)(C ₆ Cl ₄ O ₂)P(Ph)][B(C ₆ F ₅) ₄] ₂ (3)	4
2.2 Synthesis of [(terpy)(C ₆ Cl ₄ O ₂)P(Ph)][OTf] ₂ (4)	7
2.3 Synthesis of [(terpy)(C ₁₄ H ₈ O ₂)P(Ph)][B(C ₆ F ₅) ₄] ₂ (5)	9
2.4 Synthesis of [(terpy)(C ₁₄ H ₈ O ₂)P(Ph)][OTf] ₂ (6).....	12
3. Gutmann-Beckett test for 3	14
3.1 Reaction of 3 with Et ₃ PO	14
4. Hydrodefluorination (HDF) catalysis	15
4.1 General procedure	15
4.2 HDF of (trifluoromethyl)cyclohexane, (<i>c</i> -C ₆ H ₁₁)CF ₃	15
4.3 HDF of fluoroheptane, <i>n</i> -C ₇ H ₁₅ F	17
4.4 HDF of 4-bromo- α,α,α -trifluorotoluene, (<i>p</i> -BrC ₆ H ₄)CF ₃	18
5. Computations	19
5.1 Calculations of the HOMO and LUMO of the cation of 3/4 and 5/6	19
5.2 Terpy-centered HDF mechanism with hydride delivery from Et ₃ SiH as the initial step.....	23
5.3 Phosphorus-centered HDF mechanism with hydride delivery from Et ₃ SiH as the initial step	25

5.4 Terpy-centered HDF mechanism with fluoride delivery from PhCF_3 as the initial step	27
5.5 Phosphorus-centered HDF mechanism with fluoride delivery from PhCF_3 as the initial step	29
6. X-ray Crystallography	31
7. References.....	32

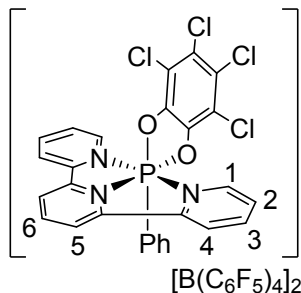
1. General Considerations

All manipulations were performed under an atmosphere of dry, oxygen-free N₂ by means of standard Schlenk or glovebox techniques (MBraun LABmaster SP dry glovebox equipped with a -35 °C freezer). Pentane and ether were collected from a Grubbs-type column system manufactured by Innovative Technology and were dried over 4 Å molecular sieves. Molecular sieves, type 4 Å (pellets, 3.2 mm diameter) purchased from Sigma Aldrich, were activated prior to usage by heating at approximately 250 °C under dynamic vacuum for 48 hours. Dichloromethane (DCM), chloroform, and acetonitrile were dried over CaH₂, followed by distillation and degassing. Acetonitrile-d₃, purchased from Cambridge Isotope Laboratories, was degassed and dried over calcium hydride. Unless otherwise mentioned, reagents were purchased from Sigma Aldrich or TCI America and used without further purification. [(terpy)P(Ph)][B(C₆F₅)₄]₂ (**1**) and [(terpy)P(Ph)][OTf]₂ (**2**) were prepared using literature methods.^[1]

NMR spectra were recorded on a Bruker Avance III 400 MHz spectrometer. Spectra were referenced to residual solvent of CD₃CN (¹H = 1.94 ppm; ¹³C = 1.32 ppm), or externally (¹¹B: (Et₂O)BF₃ (δ 0.00), ¹⁹F: CFC₃ (δ 0.00), ³¹P: 85% H₃PO₄ (δ 0.00)). All spectra were obtained at 298 K. Chemical shifts (δ) are reported in ppm and the absolute values of the coupling constants (*J*) are in Hz, while the multiplicity of the signals is indicated as “s”, “d”, “t”, or “m” for singlet, doublet, triplet, or multiplet, respectively. In some instances, signal and/or coupling assignment was derived from 2D NMR experiments. Combustion analyses were performed in-house employing a Flash 2000 from Thermo Instruments CHN Analyzer.

2. Synthesis of P(V) Compounds

2.1 Synthesis of [(terpy)(C₆Cl₄O₂)P(Ph)][B(C₆F₅)₄]₂ (**3**)



At room temperature, a solution of *o*-chloranil (13.8 mg, 0.0561 mmol) in DCM (2 mL) was added dropwise to a solution of [(terpy)P(Ph)][B(C₆F₅)₄]₂, **1**, (86.4 mg, 0.0508 mmol) in DCM (2 mL) while stirring. The solution was stirred for 24 hours, and all volatiles were removed *in vacuo*. The residue was washed with chloroform (3 x 5 mL), and the remaining solid was dried *in vacuo* to give **3** as a red powder (92.0 mg, 93 % yield).

¹H NMR (400 MHz, CD₃CN): δ 9.29 (t, *J* = 8 Hz, 1H, H₆), 9.20 (dd, *J* = 8 Hz, *J* = 3 Hz, 2H, H₅), 9.05 (t, *J* = 5 Hz, 2H, H₁), 9.00 (d, *J* = 8 Hz, 2H, H₄), 8.76 (t, *J* = 8 Hz, 2H, H₃), 8.18 (tm, *J* = 7 Hz, 2H, H₂), 7.33-7.12 (m, 5H, *Ph*).

¹³C{¹H} NMR (125 MHz, CD₃CN): δ ([B(C₆F₅)₄ peaks not included) 152.9 (s), 148.8 (s), 144.6 (s), 143.8 (s), 140.9 (d, *J* = 5 Hz), 139.9 (d, *J* = 5 Hz), 137.3 (d, *J* = 5 Hz), 133.5 (s), 132.7 (d, *J* = 4 Hz), 131.2 (d, *J* = 12 Hz), 131.0 (d, *J* = 20 Hz), 130.2 (s), 129.7 (s), 129.5 (s), 129.4 (s), 129.3 (s), 128.4 (s), 127.4 (s), 127.0 (s).

³¹P{¹H} NMR (162 MHz, CD₃CN): δ -104.8 (s).

¹⁹F{¹H} NMR (376 MHz, CD₃CN): δ -133.7 (m, 8F, *o*-C₆F₅), -163.9 (t, 4F, ³*J*_{FF} = 20 Hz, *p*-C₆F₅), -168.3 (s, 8F, *m*-C₆F₅).

¹¹B{¹H} NMR (128 MHz, CD₃CN): δ -16.7 (s).

Anal. Calc. for C₇₅H₁₆B₂Cl₄F₄₀N₃O₂P: C 46.31 %, H 0.83 %, N 2.16 %. Found: C 46.08 %, H 1.06 %, N 2.49 %.

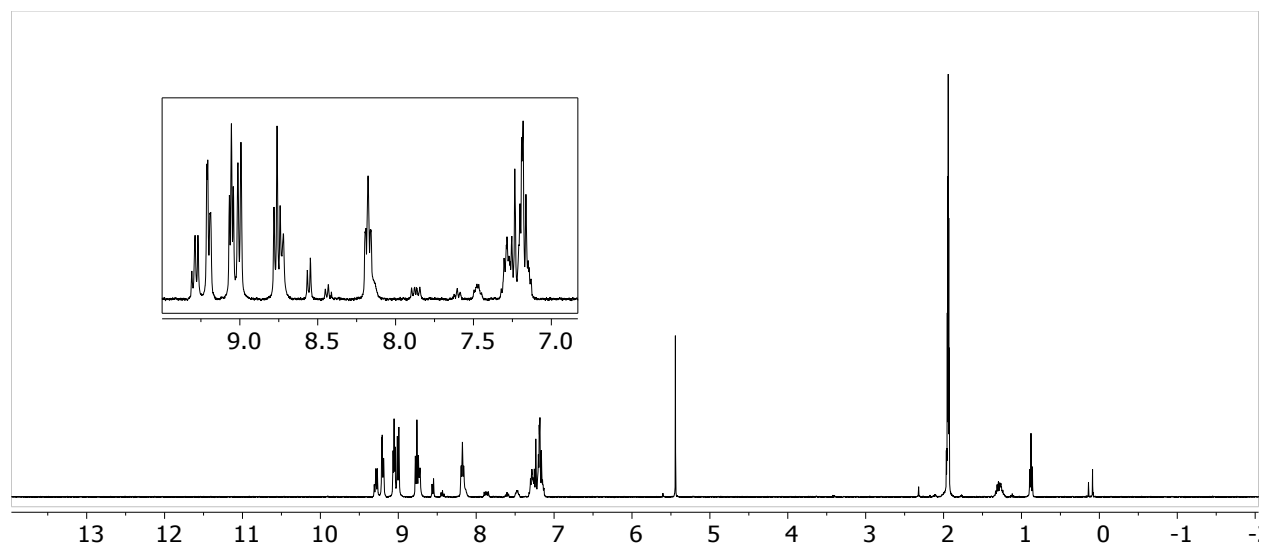


Figure S1. ^1H NMR spectrum of **3**

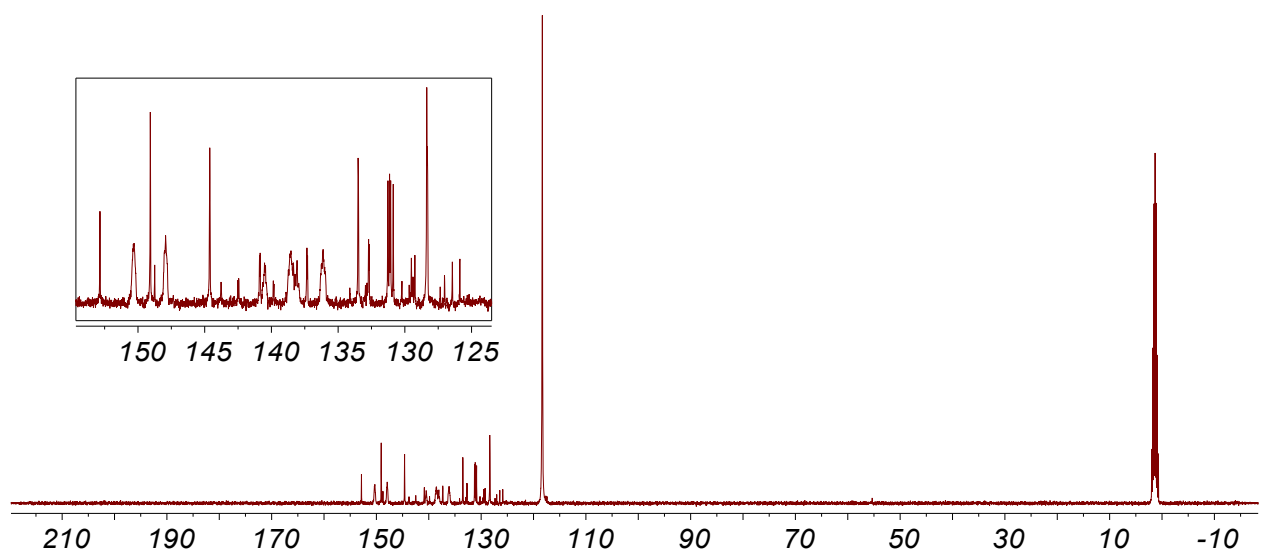


Figure S2. $^{13}\text{C}\{^1\text{H}\}$ NMR spectrum of **3**

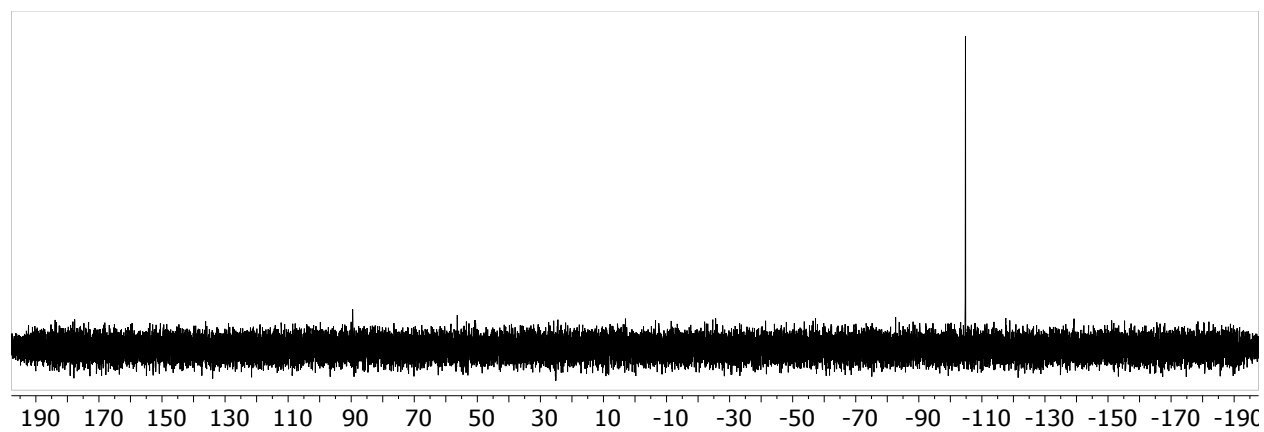


Figure S3. $^{31}\text{P}\{^1\text{H}\}$ NMR spectrum of **3**

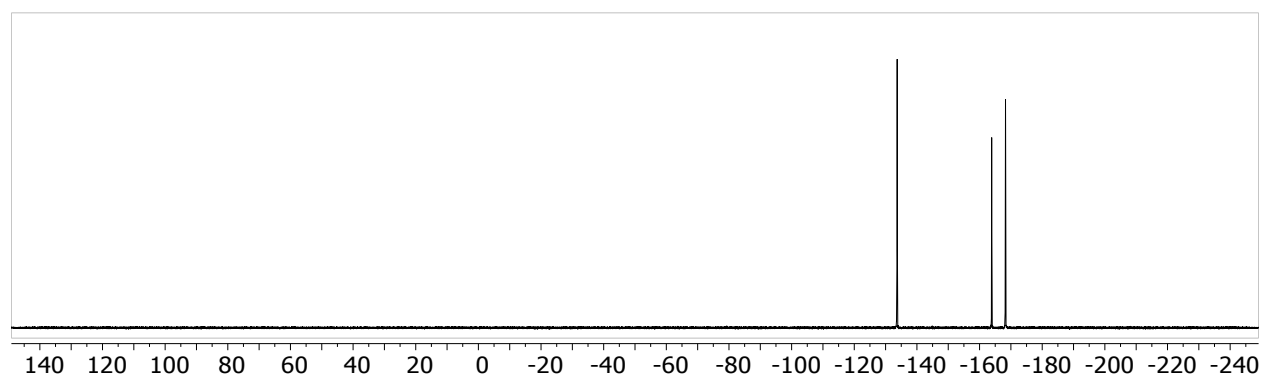


Figure S4. $^{19}\text{F}\{^1\text{H}\}$ NMR spectrum of **3**

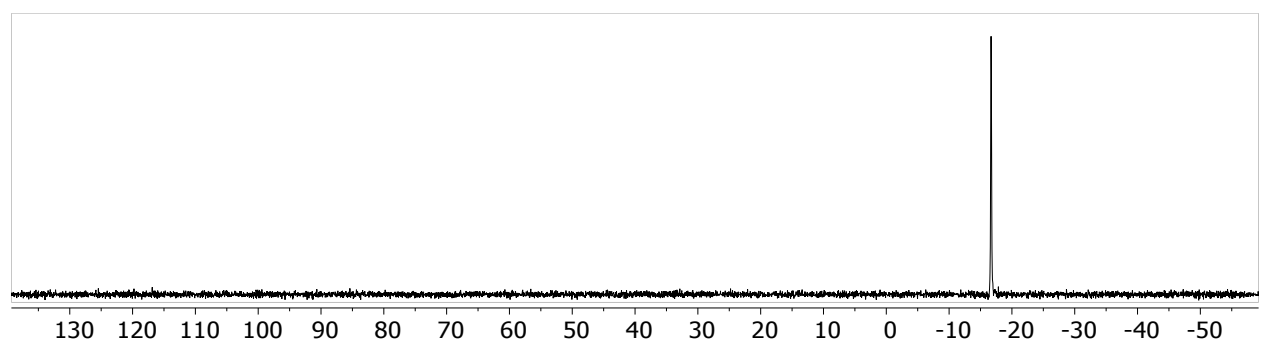
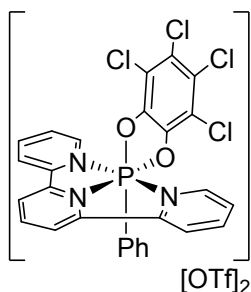


Figure S5. $^{11}\text{B}\{^1\text{H}\}$ NMR spectrum of **3**

2.2 Synthesis of [(terpy)(C₆Cl₄O₂)P(Ph)][OTf]₂ (**4**)



At room temperature, a solution of *o*-chloranil (27.9 mg, 0.113 mmol) in CH₃CN (3 mL) was added dropwise to a solution of [(terpy)P(Ph)][OTf]₂, **2**, (49.1 mg, 0.0768 mmol) in CH₃CN (2 mL) while stirring. The solution was stirred for 24 hours, and all volatiles were removed *in vacuo*. The residue was washed with DCM (3 x 5 mL), and the remaining solid was dried *in vacuo* to give **4** as a red powder (62.4 mg, 92 % yield). Single crystals suitable for X-ray diffraction were obtained by layering a solution of **4** in CH₃CN with ether and placing in the freezer at -35 °C.

¹H NMR (400 MHz, CD₃CN): δ 9.34-9.27 (m, 3H), 9.10-9.04 (m, 4H), 8.78 (t, ³J_{HH} = 8 Hz, 2H), 8.23-8.17 (tm, ³J_{HH} = 8 Hz, 2H), 7.35-7.18 (m, 5H).

¹³C{¹H} NMR (125 MHz, CD₃CN): δ 152.8 (d, J_{CP} = 1 Hz), 149.1 (d, J_{CP} = 1 Hz), 144.6 (d, J_{CP} = 2 Hz), 142.3 (s), 140.8 (d, J_{CP} = 5 Hz), 140.7 (s), 139.9 (d, J_{CP} = 5 Hz), 137.3 (d, J_{CP} = 5 Hz), 133.5 (d, J_{CP} = 3 Hz), 132.7 (d, J_{CP} = 5 Hz), 131.3 (d, J_{CP} = 12 Hz), 131.0 (d, J_{CP} = 20 Hz), 129.4 (s), 128.5 (d, J_{CP} = 6 Hz), 128.5 (d, J_{CP} = 1 Hz), 126.9 (s), 122.1 (q, ¹J_{CF} = 321 Hz, OTf), 117.5 (d, J_{CP} = 22 Hz).

³¹P{¹H} NMR (162 MHz, CD₃CN): δ -104.8 (s).

¹⁹F{¹H} NMR (376 MHz, CD₃CN): δ -79.2 (s).

Anal. Calc. for C₂₉H₁₆Cl₄F₆N₃O₈PS₂: C 39.34 %, H 1.82 %, N 4.75 %. Found: C 39.65 %, H 1.88%, N 4.95 %.

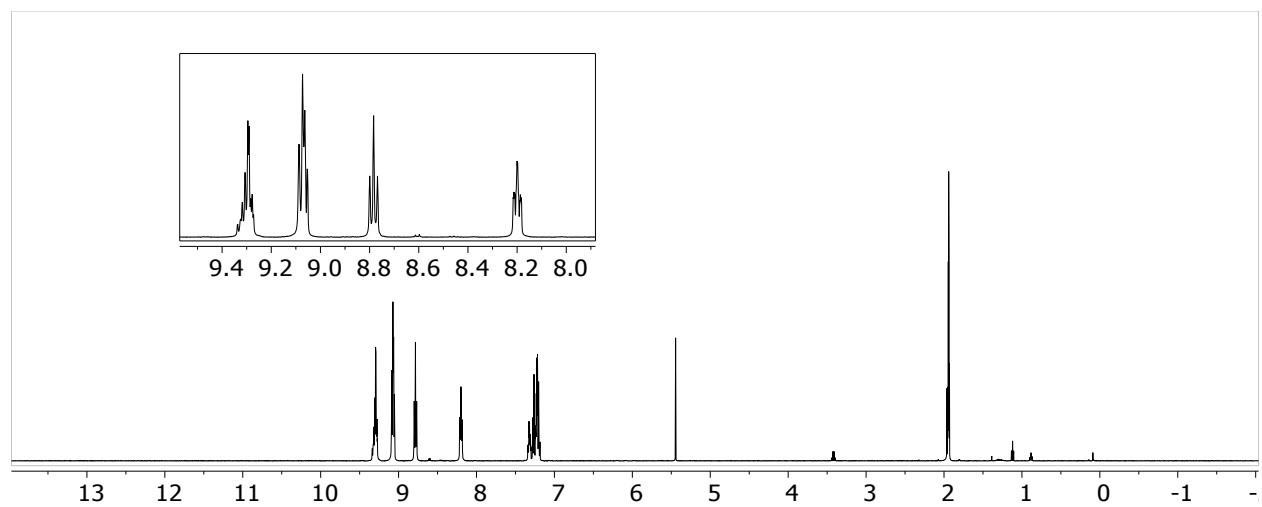


Figure S6. ^1H NMR spectrum of **4**

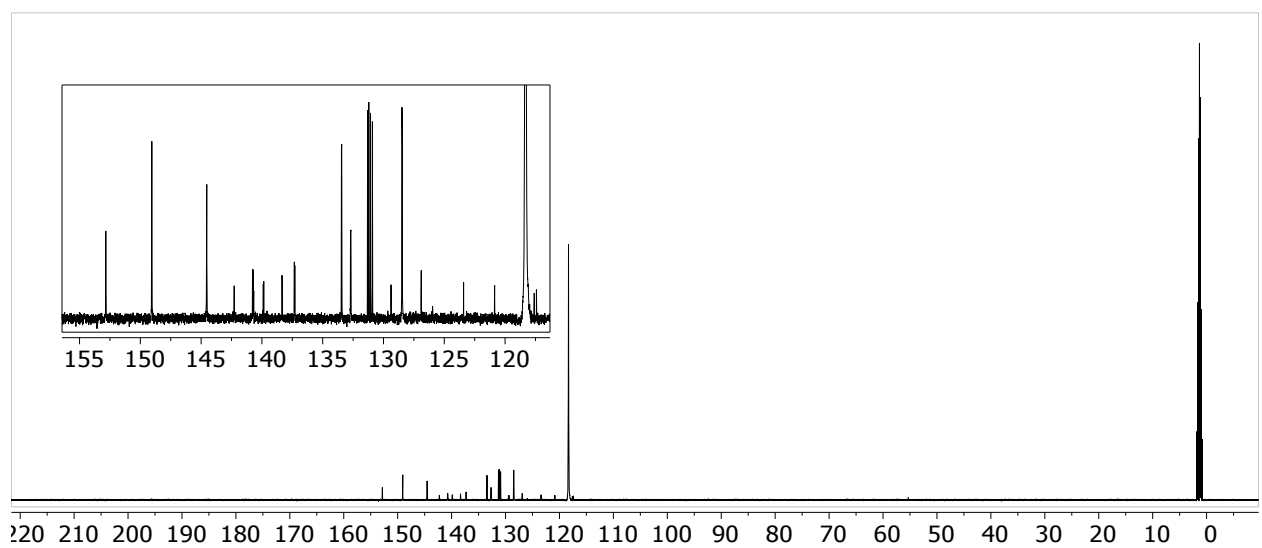


Figure S7. $^{13}\text{C}\{^1\text{H}\}$ NMR spectrum of **4**

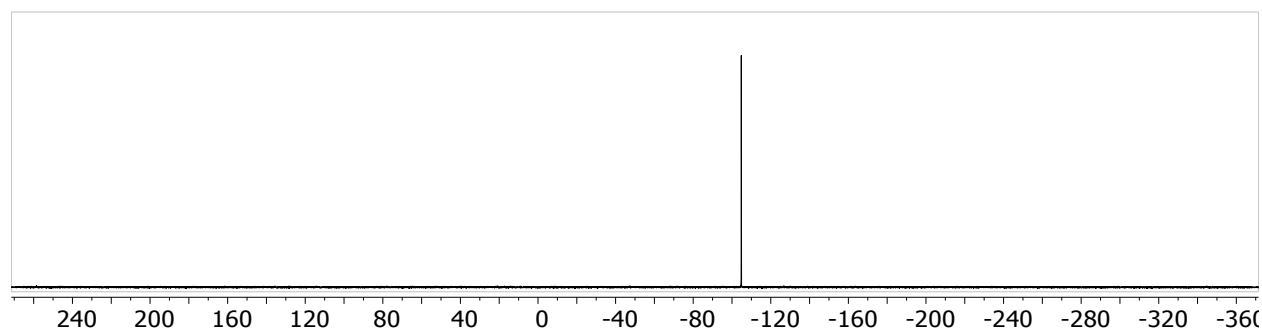


Figure S8. $^{31}\text{P}\{^1\text{H}\}$ NMR spectrum of **4**

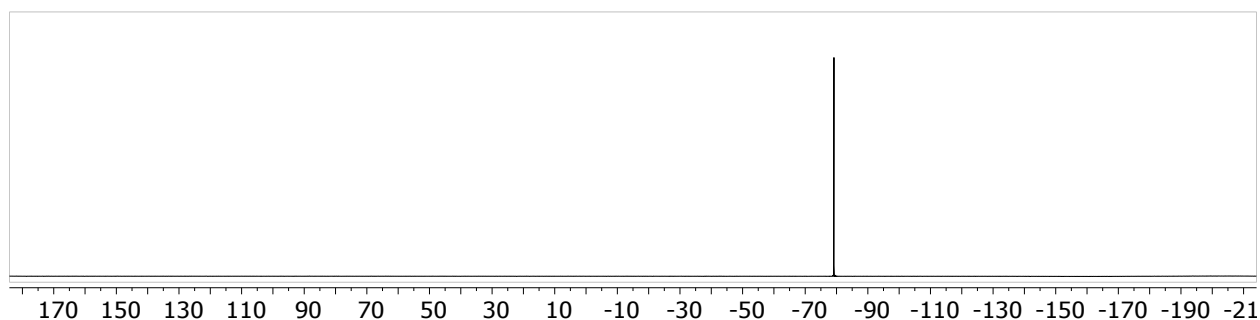
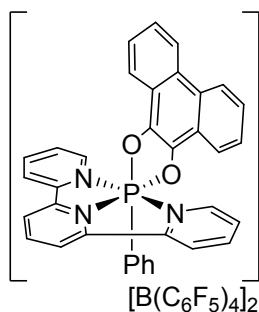


Figure S9. $^{19}\text{F}\{^1\text{H}\}$ NMR spectrum of **4**

2.3 Synthesis of $[(\text{terpy})(\text{C}_{14}\text{H}_8\text{O}_2)\text{P}(\text{Ph})][\text{B}(\text{C}_6\text{F}_5)_4]_2$ (**5**)



At room temperature, a solution of 9,10-phenanthrenequinone (5.0 mg, 0.024 mmol) in DCM (2 mL) was added dropwise to a solution of $[(\text{terpy})\text{P}(\text{Ph})][\text{B}(\text{C}_6\text{F}_5)_4]_2$, **1**, (37.2 mg, 0.0219 mmol) in DCM (2 mL) while stirring. The solution was stirred for 12 hours, and all volatiles were removed *in vacuo*. The residue was washed with chloroform (2 x 0.5 mL) and pentane (3 x 2 mL), and the remaining solid was dried *in vacuo* to give **5** as a red powder (37.2 mg, 89 % yield). Compound **5** proved to be unstable for extended periods of time in both the solid state and in solution, and decomposed into unidentifiable products. As such, ^1H , $^{13}\text{C}\{^1\text{H}\}$, and $^{31}\text{P}\{^1\text{H}\}$ NMR spectra of the completely pure **5** could not be obtained. The reported chemical shifts for the ^1H and $^{13}\text{C}\{^1\text{H}\}$ NMR spectra below correlate to those seen in the spectra, though they are not all assigned to compound **5**. The $^{31}\text{P}\{^1\text{H}\}$ NMR spectrum of the sample after 24 hours can be seen in Figure S15.

^1H NMR (400 MHz, CD_3CN): δ 9.33-9.13 (m, 4H), 8.98 (d, $J = 8$ Hz, 1.5H), 8.83 (d, $J = 9$ Hz, 2H), 8.75-8.62 (m, 4H), 8.62-8.52 (m, 2H), 8.36-8.25 (m, 2H), 8.16-7.92 (m, 5.5H), 7.82-7.76 (m, 1H), 7.62-7.16 (m, 10H).

$^{13}\text{C}\{^1\text{H}\}$ NMR (125 MHz, CD_3CN): δ ($[\text{B}(\text{C}_6\text{F}_5)_4]$ peaks not included) 152.0 (s), 149.1 (s), 148.4 (d, $J = 8$ Hz), 147.1 (s), 147.0 (s), 144.4 (s), 143.9 (s), 143.2 (d, $J = 11$ Hz), 142.4 (s), 142.3 (s), 141.1 (d, $J = 4$ Hz), 137.8 (d, $J = 4$ Hz), 134.5 (d, $J = 3$ Hz), 132.9 (m), 132.6 (d, $J = 2$ Hz), 132.3

(d, $J = 4$ Hz), 131.5 (d, $J = 12$ Hz), 130.8 (d, $J = 19$ Hz), 130.6 (s), 130.0 (m), 129.4 (s), 129.3-128.8 (m), 128.6 (s), 128.1 (s), 128.0 (d, $J = 3$ Hz), 127.8-127.3 (m), 126.4 (s), 125.9 (s), 125.6 (s), 124.7 (d, $J = 8$ Hz), 124.4 (d, $J = 10$ Hz), 122.3-122.0 (m).

$^{31}\text{P}\{^1\text{H}\}$ NMR (162 MHz, CD_3CN): δ -102.0 (s).

$^{19}\text{F}\{^1\text{H}\}$ NMR (376 MHz, CD_3CN): δ -133.7 (m, 8F, *o*- C_6F_5), -163.8 (t, 4F, $^3J_{\text{FF}} = 21$ Hz, *p*- C_6F_5), -168.3 (s, 8F, *m*- C_6F_5).

^{11}B NMR (128 MHz, CD_3CN): δ -16.7 (s).

Anal. Calc. for $\text{C}_{42}\text{H}_{34}\text{BClF}_4\text{N}_2\text{P}_2$: C 52.26 %, H 1.27 %, N 2.20 %. Found: C 54.03 %, H 1.76 %, N 2.03 %.

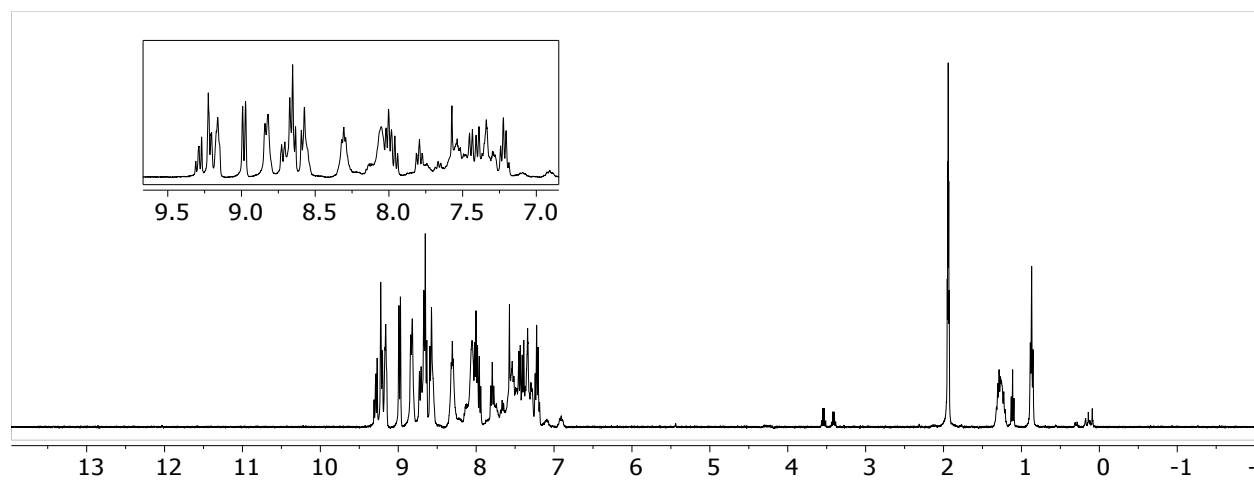


Figure S10. ^1H NMR spectrum of **5**

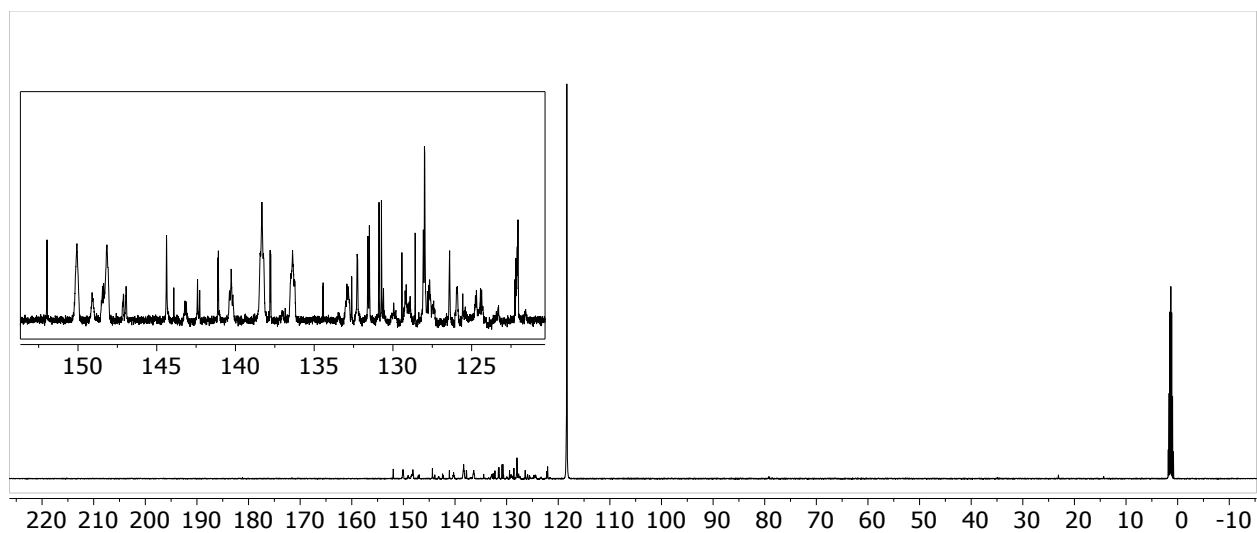


Figure S11. $^{13}\text{C}\{^1\text{H}\}$ NMR spectrum of **5**

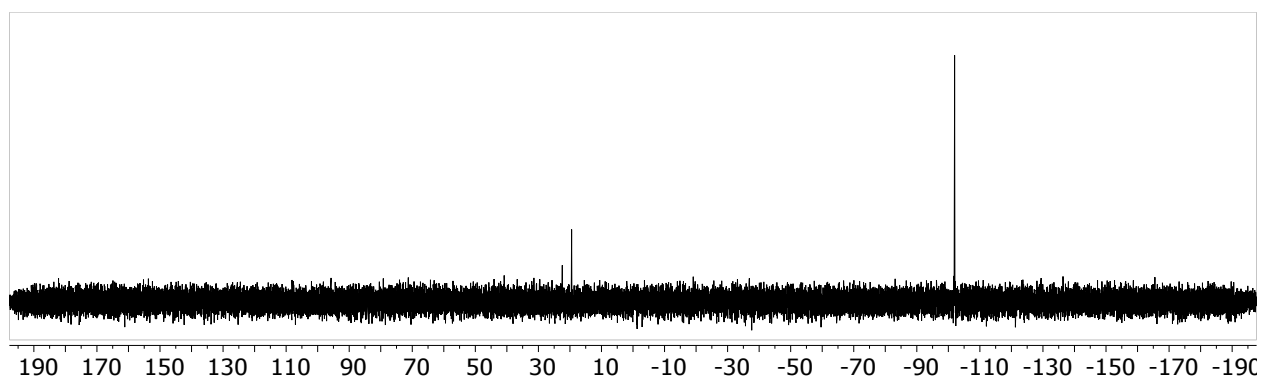


Figure S12. $^{31}\text{P}\{^1\text{H}\}$ NMR spectrum of **5**

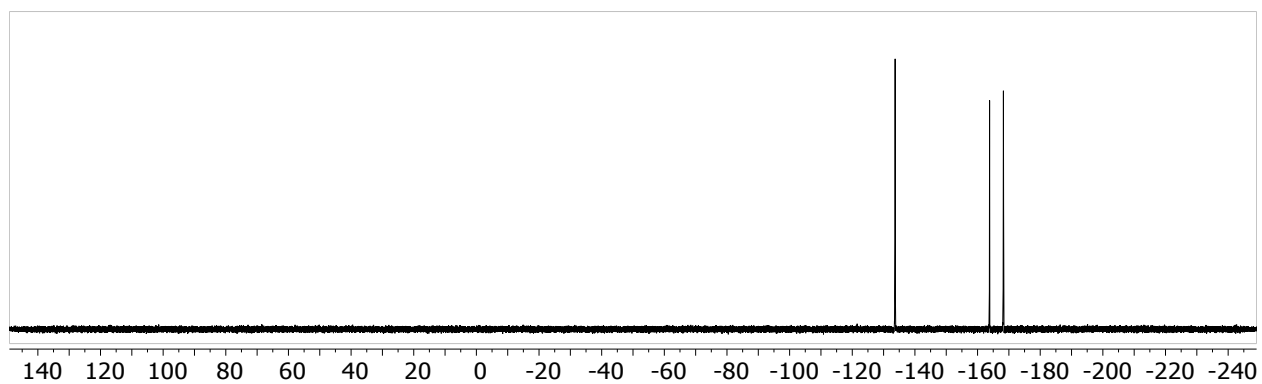


Figure S13. $^{19}\text{F}\{^1\text{H}\}$ NMR spectrum of **5**

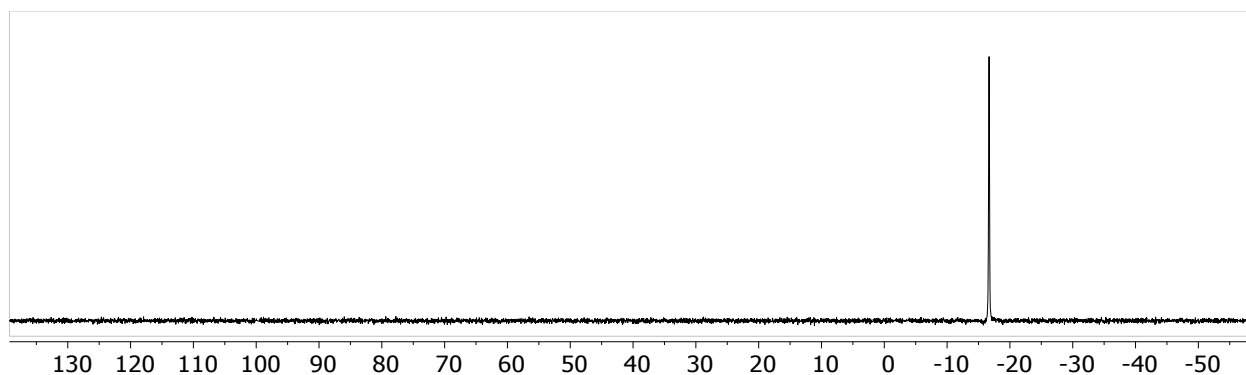


Figure S14. $^{11}\text{B}\{^1\text{H}\}$ NMR spectrum of **5**

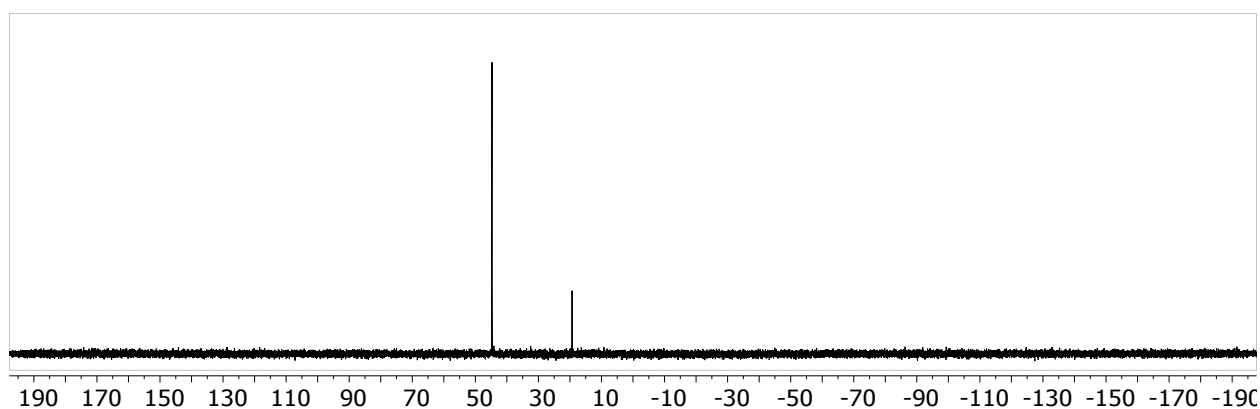
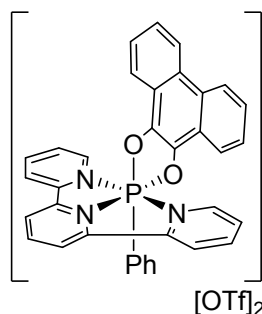


Figure S15. $^{31}\text{P}\{^1\text{H}\}$ NMR spectrum of **5** after 24 hours

2.4 Synthesis of $[(\text{terpy})(\text{C}_{14}\text{H}_8\text{O}_2)\text{P}(\text{Ph})][\text{OTf}]_2$ (**6**)



At room temperature, a solution of 9,10-phenanthrenequinone (8.2 mg, 0.394 mmol) in CH_3CN (3 mL) was added dropwise to a solution of $[(\text{terpy})\text{P}(\text{Ph})][\text{OTf}]_2$, **2**, (24.8 mg, 0.0388 mmol) in CH_3CN (2 mL) while stirring. The solution was stirred for 12 hours, and all volatiles were removed *in vacuo*. The residue was washed with DCM (3 x 1 mL) and pentane (3 x 1 mL), and the remaining solid was dried *in vacuo* to give **6** as a red powder (30.9 mg, 94 % yield). Single crystals suitable

for X-ray diffraction were obtained by layering a solution of **6** in CH₃CN with ether and placing in the freezer at -35 °C. Since **6** was prepared solely for the purpose of obtaining single crystals, only the ³¹P{¹H} and ¹⁹F{¹H} NMR spectra were obtained to confirm the product.

³¹P{¹H} NMR (162 MHz, CD₃CN): δ -101.7 (s).

¹⁹F{¹H} NMR (376 MHz, CD₃CN): δ -79.2 (s).

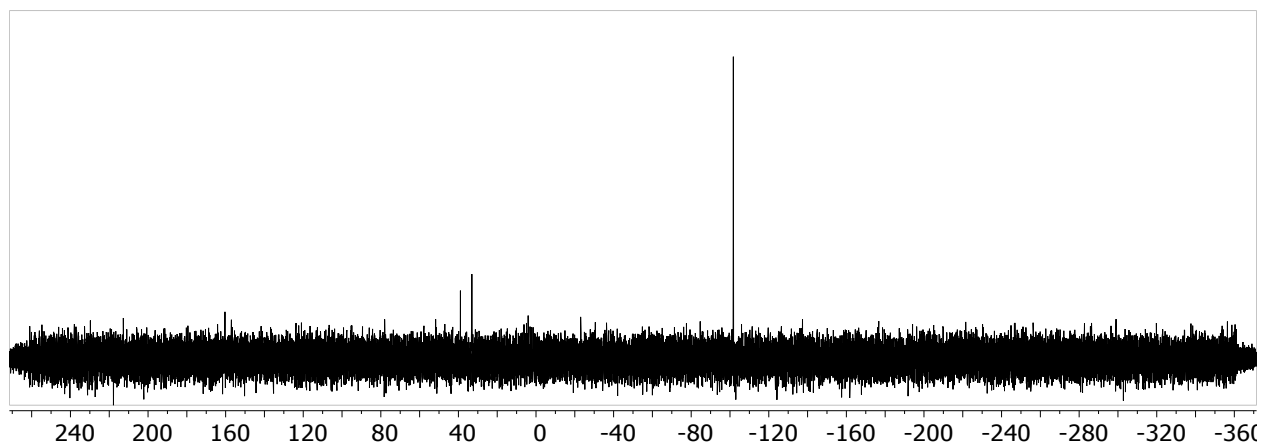


Figure S16. ³¹P{¹H} NMR spectrum of **6**

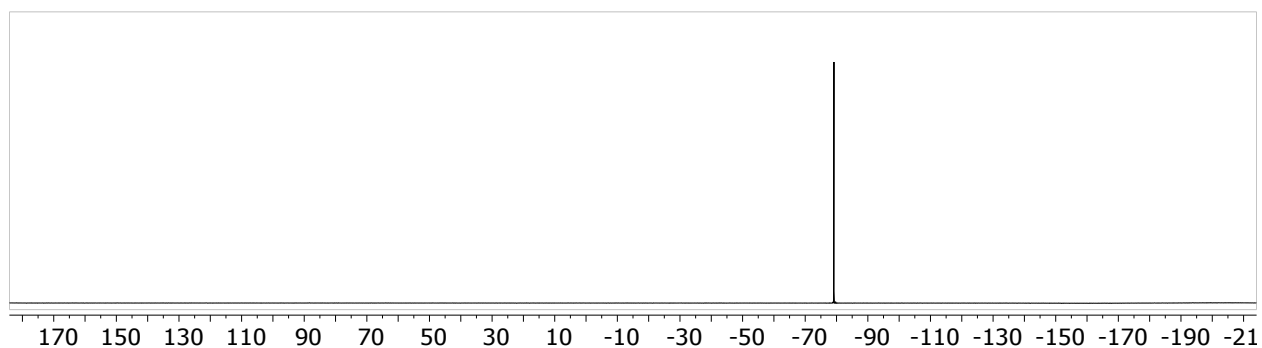


Figure S17. ¹⁹F{¹H} NMR spectrum of **6**

3. Gutmann-Beckett test for **3**

3.1 Reaction of **3** with Et₃PO

Compound **3** (18.1 mg, 0.00930 mmol) and triethylphosphine oxide (1.2 mg, 0.0089 mmol) were dissolved in DCM (0.5 mL). After 15 minutes, the ³¹P{¹H} NMR spectrum of the reaction mixture was obtained.

³¹P{¹H} NMR (162 MHz, DCM): δ 55.8 (br s), -103.1 (s).

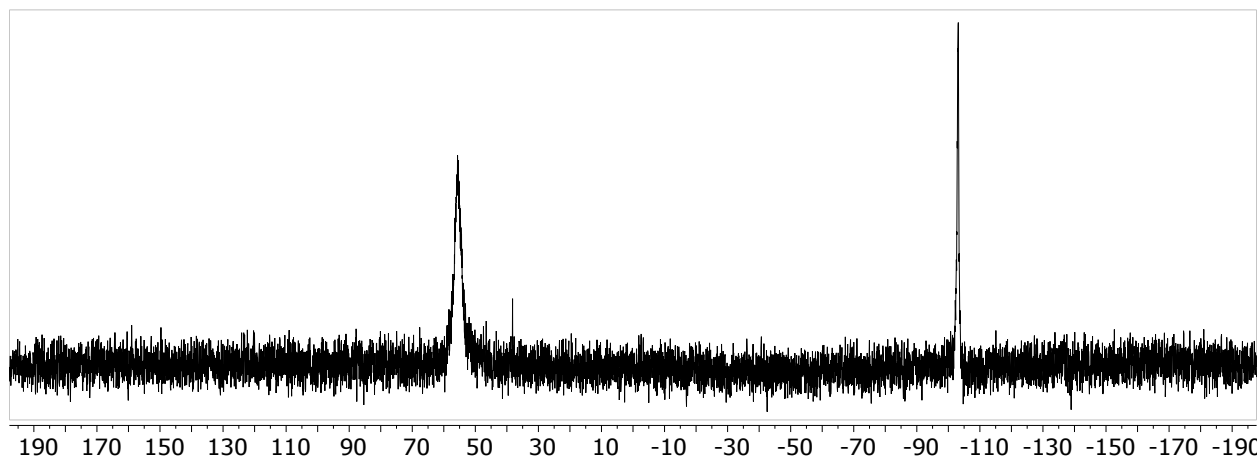
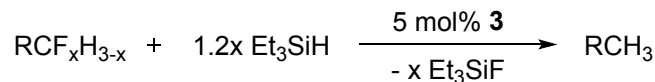


Figure S18. ³¹P{¹H} NMR spectrum of the reaction mixture of **3** and Et₃PO in DCM.

4. Hydrodefluorination (HDF) catalysis

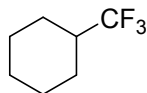
4.1 General procedure



At room temperature, the corresponding fluoroalkane (1 equivalent) and triethylsilane (1.2 equivalents per CF bond) were dissolved in DCM (1 mL) and transferred to an NMR tube containing a sealed capillary containing C₆F₆ and mesitylene dissolved in CDCl₃. Initial NMR spectra were obtained. Compound **3*** (0.05 equivalents) was added as a solid to the solution, which marked t = 0 h. The reaction progress was monitored by ¹H and ¹⁹F{¹H} NMR spectroscopy; the ³¹P{¹H} NMR spectra generally did not exhibit any signals due to the low concentration of catalyst. The NMR yield was determined by ¹⁹F{¹H} NMR spectroscopy; the ratio of the generated Et₃SiF peak to the C₆F₆ peak was calculated, which was then compared to the initial ratio of the fluoroalkane peak to the C₆F₆ peak at t = 0 h. This provided the value for the percent yield based on the amount of Et₃SiF generated.

*Compound **3** was freshly prepared and its purity confirmed by spectroscopy prior to catalysis.

4.2 HDF of (trifluoromethyl)cyclohexane, (*c*-C₆H₁₁)CF₃



(*c*-C₆H₁₁)CF₃ (6.3 mg, 0.041 mmol), Et₃SiH (18.3 mg, 0.157 mmol), and **3** (4.1 mg, 0.0021 mmol) were used. The ¹⁹F{¹H} NMR spectrum indicated 87 % conversion from (*c*-C₆H₁₁)CF₃ (-77.5 ppm) to (*c*-C₆H₁₁)CH₃ and Et₃SiF (-179.0 ppm) at t = 13 h.

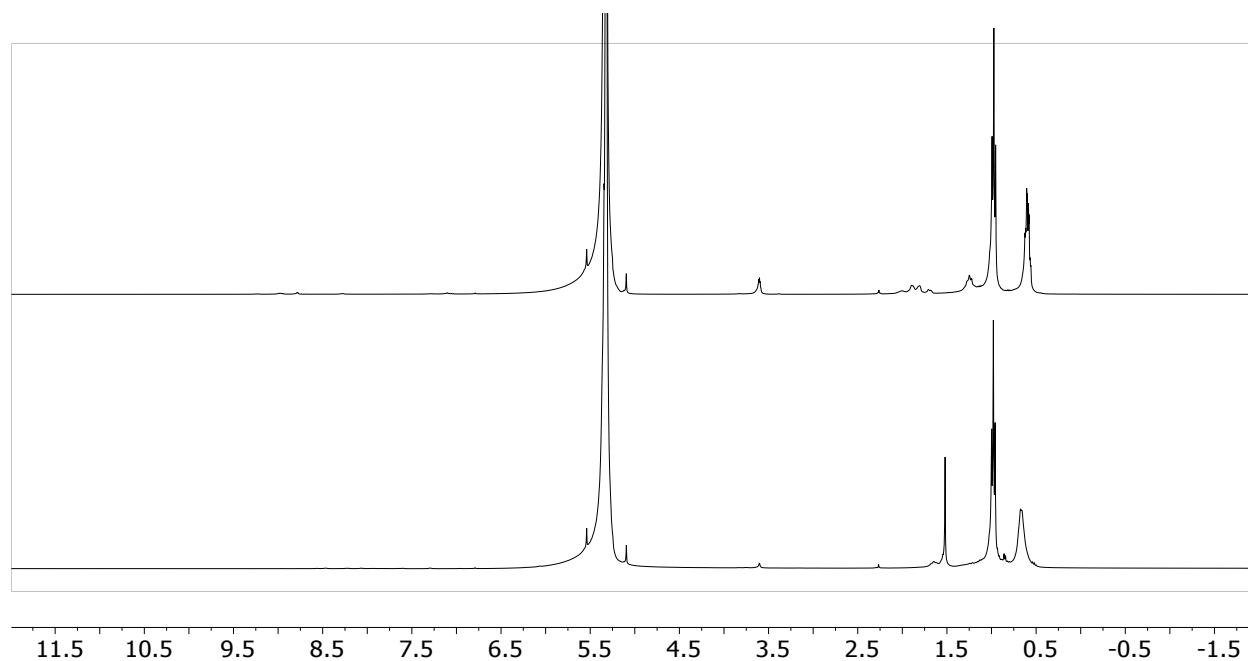


Figure S19. ^1H NMR spectrum of the reaction mixture at $t = 0$ h (top) and $t = 13$ h (bottom).

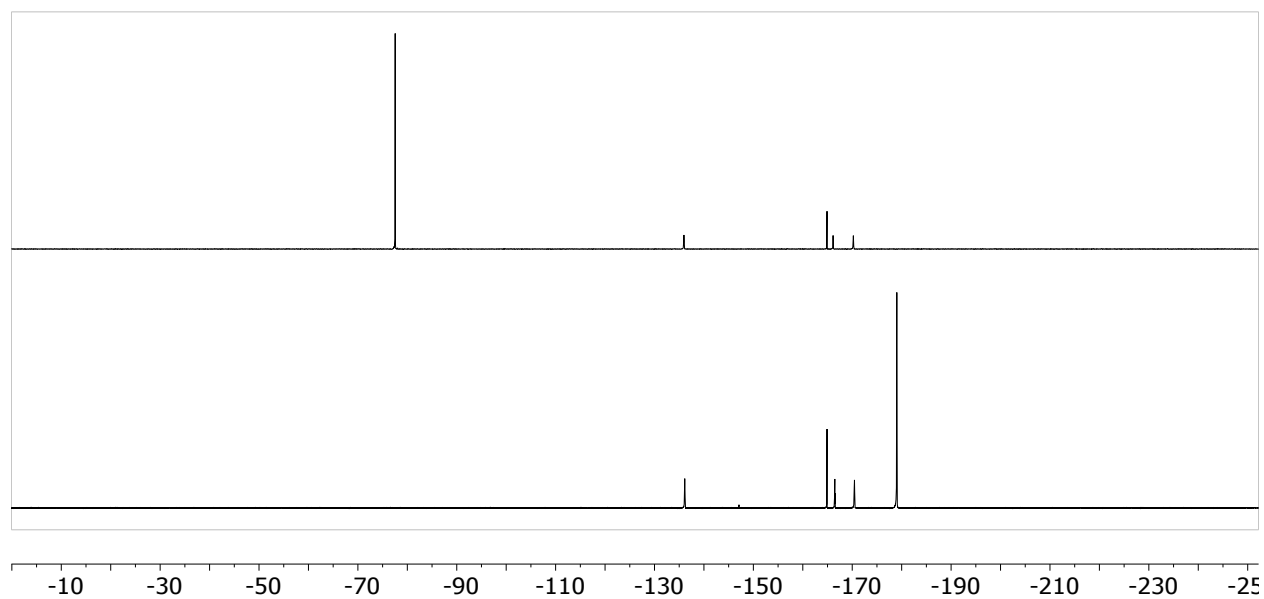
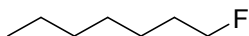


Figure S20. $^{19}\text{F}\{^1\text{H}\}$ NMR spectrum of the reaction mixture at $t = 0$ h (top) and $t = 13$ h (bottom).

4.3 HDF of fluoroheptane, $n\text{-C}_7\text{H}_{15}\text{F}$



$n\text{-C}_7\text{H}_{15}\text{F}$ (5.2 mg, 0.044 mmol), Et_3SiH (6.2 mg, 0.053 mmol), and **3** (4.3 mg, 0.0022 mmol) were used. The $^{19}\text{F}\{^1\text{H}\}$ NMR spectrum indicated 88 % conversion from $n\text{-C}_7\text{H}_{15}\text{F}$ (-221.2 ppm) to $n\text{-C}_7\text{H}_{16}$ and Et_3SiF (-179.0 ppm) at $t = 3$ h.

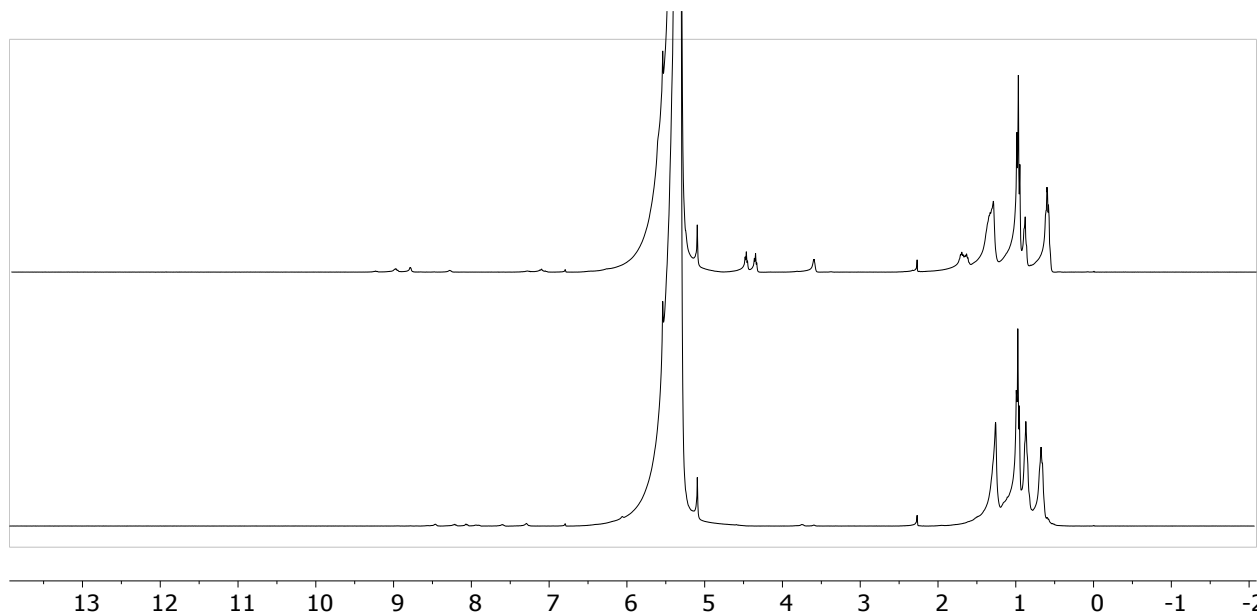


Figure S21. ^1H NMR spectrum of the reaction mixture at $t = 0$ h (top) and $t = 3$ h (bottom).

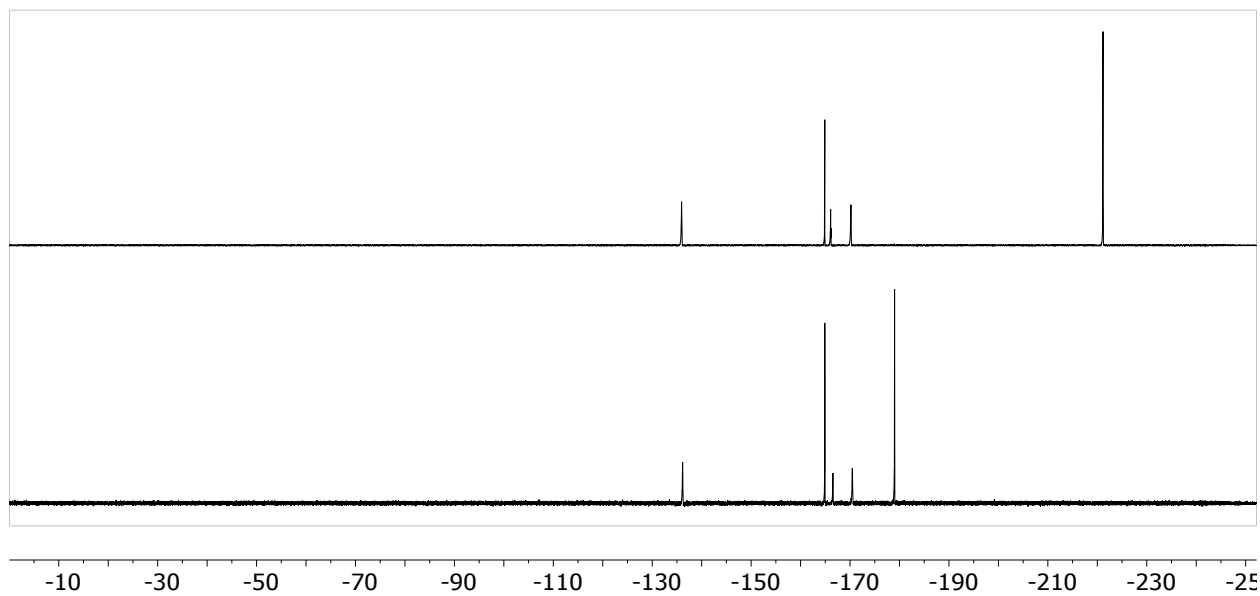
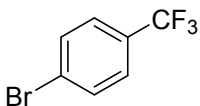


Figure S22. $^{19}\text{F}\{^1\text{H}\}$ NMR spectrum of the reaction mixture at $t = 0$ h (top) and $t = 3$ h (bottom).

4.4 HDF of 4-bromo- α,α,α -trifluorotoluene, (p -BrC₆H₄)CF₃



(p -BrC₆H₄)CF₃ (8.9 mg, 0.040 mmol), Et₃SiH (6.0 mg, 0.052 mmol), and **3** (3.9 mg, 0.0020 mmol) were used. The ¹⁹F{¹H} NMR spectrum indicated 31 % conversion from (p -BrC₆H₄)CF₃ (-66.2 ppm) to (p -BrC₆H₄)CH₃ and Et₃SiF (-179.0 ppm) at $t = 24$ h.

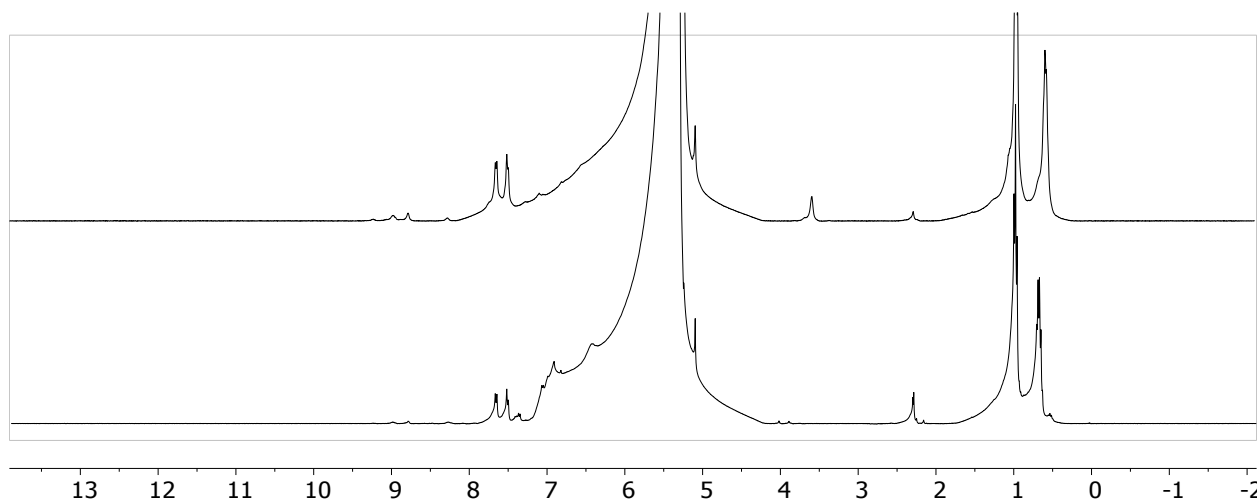


Figure S23. ¹H NMR spectrum of the reaction mixture at $t = 0$ h (top) and $t = 24$ h (bottom).

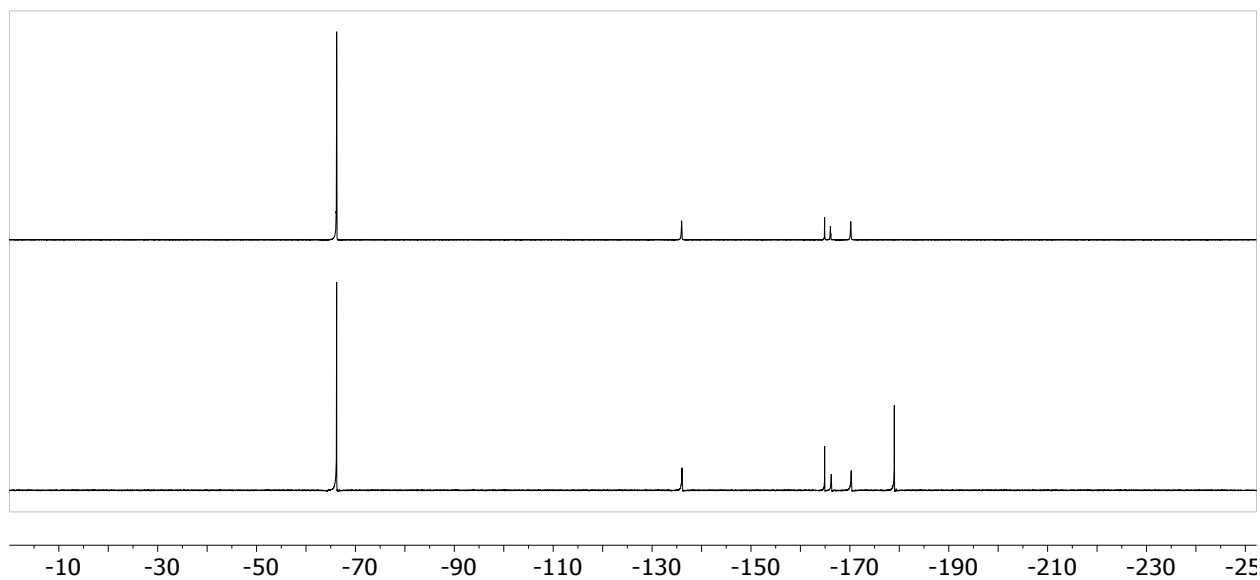


Figure S24. ¹⁹F{¹H} NMR spectrum of the reaction mixture at $t = 0$ h (top) and $t = 24$ h (bottom).

5. Computations

5.1 Calculations of the HOMO and LUMO of the cation of 3/4 and 5/6

All computations were performed using the Gaussian 09 program.^[2] Both the geometry optimization and the NBO calculations^[3] of the cation of 3/4 and 5/6 were performed at the M06-2X/def2-SVP level of theory. The stationary nature of the converged-upon geometry was confirmed by carrying out a frequency calculation and ensuring the absence of imaginary frequencies.

Table S1. Cartesian coordinates (Å) of the optimized structure of the cation of 3/4

P	-0.9439903	0.2276761	-0.0618270
N	-1.0799461	0.4014852	1.8373797
N	-2.1575347	-1.1411133	0.2278188
N	-1.0921923	-0.3676460	-1.8662195
O	0.1663821	-1.0556769	0.2015301
O	0.3063761	1.2839642	-0.2918156
C	-0.4146874	1.3106182	2.5478118
H	0.2463841	1.9682674	2.0010376
C	-0.5819925	1.3944615	3.9184736
H	-0.0253959	2.1349964	4.4764031
C	-1.4611843	0.5282624	4.5462855
H	-1.6110571	0.5797593	5.6172230
C	-2.1533288	-0.4105288	3.7916300
H	-2.8479285	-1.0940867	4.2600181
C	-1.9357102	-0.4539057	2.4310259
C	-2.5500946	-1.3771967	1.4810282
C	-3.4195190	-2.4240608	1.7325680
H	-3.7576954	-2.6346350	2.7372764
C	-3.8332003	-3.2092520	0.6648542
H	-4.5088519	-4.0371837	0.8396065
C	-3.3780944	-2.9551734	-0.6230020
H	-3.6869410	-3.5773395	-1.4511520
C	-2.5152201	-1.8922725	-0.8169665
C	-1.9010057	-1.4282225	-2.0590554
C	-2.0930555	-1.9526206	-3.3188859
H	-2.7472994	-2.8003152	-3.4689078
C	-1.4312152	-1.3662205	-4.3910613
H	-1.5623622	-1.7618453	-5.3902440
C	-0.6106683	-0.2726105	-4.1723407

H	-0.0850417	0.2094102	-4.9852839
C	-0.4618184	0.2131951	-2.8852739
H	0.1538228	1.0706537	-2.6504034
C	1.4518929	-0.6380595	0.1161272
C	2.5796933	-1.4134333	0.2838866
C	3.8259834	-0.7821002	0.1583192
C	3.9120639	0.5895065	-0.1262877
C	2.7491968	1.3547982	-0.2917235
C	1.5431607	0.7046719	-0.1645814
C	-2.2291144	1.5307295	-0.3095189
C	-1.8553316	2.8782054	-0.2998521
H	-0.8220508	3.1648438	-0.1792481
C	-2.8050360	3.8745035	-0.4643261
H	-2.4905293	4.9104463	-0.4558922
C	-4.1402248	3.5530645	-0.6446208
H	-4.8782345	4.3342142	-0.7743727
C	-4.5220782	2.2212995	-0.6626503
H	-5.5610794	1.9544533	-0.8084605
C	-3.5789051	1.2203498	-0.4949339
H	-3.9372474	0.2009275	-0.5195943
Cl	2.4139165	-3.0756969	0.6308522
Cl	5.2442626	-1.7018548	0.3570423
Cl	5.4308656	1.3443380	-0.2743947
Cl	2.7735417	3.0272641	-0.6354262

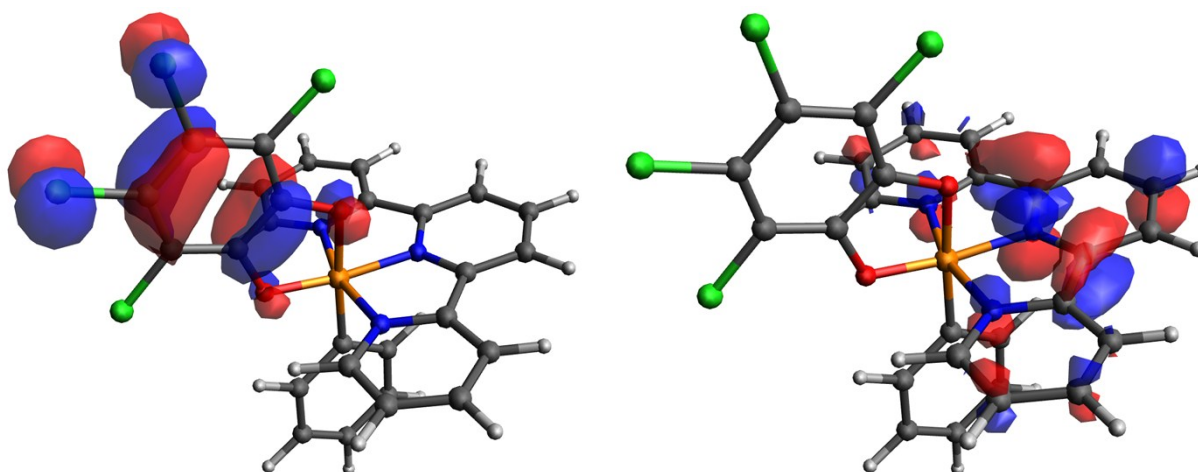


Figure S25. HOMO (left) and LUMO (right) of the cation of 3/4.

Table S2. Cartesian coordinates (Å) of the optimized structure of the cation of **5/6**

P	-0.8112274	0.2240052	0.0909984
N	-0.9326882	-0.5511964	1.8282215
N	-2.0724449	-1.0895046	-0.2985450
N	-0.9849882	0.5635345	-1.7885916
O	0.2738945	-1.0261972	-0.3079648
O	0.4283141	1.2592068	0.4002275
C	-0.2382804	-0.1046122	2.8718843
H	0.3750538	0.7703419	2.7060618
C	-0.3219066	-0.7456885	4.0964133
H	0.2546569	-0.3717514	4.9312619
C	-1.1418203	-1.8530291	4.2242483
H	-1.2223327	-2.3687915	5.1726476
C	-1.8673440	-2.3011200	3.1260766
H	-2.5197387	-3.1596256	3.2065393
C	-1.7369983	-1.6274476	1.9316583
C	-2.4164399	-1.9363505	0.6741652
C	-3.3330444	-2.9375615	0.4095382
H	-3.6315021	-3.6347585	1.1796600
C	-3.8621647	-3.0248181	-0.8722035
H	-4.5844917	-3.7981942	-1.1012879
C	-3.4646852	-2.1412281	-1.8661906
H	-3.8607158	-2.2223521	-2.8685295
C	-2.5343363	-1.1670084	-1.5468674
C	-1.9070030	-0.1835239	-2.4261039
C	-2.1552506	-0.0108919	-3.7712216
H	-2.9058567	-0.6056859	-4.2730454
C	-1.4153762	0.9363879	-4.4676810
H	-1.5878399	1.0883709	-5.5254989
C	-0.4527034	1.6742815	-3.8005240
H	0.1519910	2.4082093	-4.3153237
C	-0.2615354	1.4675698	-2.4456276
H	0.4694661	2.0173737	-1.8700412
C	1.6721516	0.6725692	0.2099409
C	2.8970450	1.3449839	0.4062364
C	2.9732965	2.6825865	0.8221888
H	2.0603077	3.2341478	1.0112127
C	4.1984407	3.2785837	0.9915981
H	4.2631830	4.3100359	1.3133493
C	5.3648165	2.5475309	0.7479537

H	6.3306530	3.0175070	0.8813338
C	5.2997669	1.2353546	0.3411661
H	6.2240573	0.7041059	0.1641503
C	4.0705810	0.5840802	0.1549755
C	3.9719384	-0.8015516	-0.2728363
C	5.1021742	-1.5933005	-0.5318047
H	6.0919614	-1.1756086	-0.4152424
C	4.9858891	-2.9026265	-0.9345656
H	5.8793168	-3.4832682	-1.1251307
C	3.7281997	-3.4905590	-1.1004415
H	3.6513005	-4.5224296	-1.4181688
C	2.5962766	-2.7532371	-0.8593309
H	1.6133973	-3.1901228	-0.9832725
C	2.7038569	-1.4174015	-0.4479894
C	1.5721345	-0.6098717	-0.1866770
C	-2.0964785	1.5005574	0.4654900
C	-3.3680922	1.1742547	0.9366842
H	-3.6611594	0.1508389	1.1283310
C	-4.3071432	2.1606636	1.1924633
H	-5.2852884	1.8833599	1.5643513
C	-3.9960549	3.4931983	0.9750982
H	-4.7303060	4.2635477	1.1729817
C	-2.7353045	3.8318693	0.5098491
H	-2.4762714	4.8703098	0.3466219
C	-1.7925136	2.8482175	0.2598717
H	-0.8108037	3.1452838	-0.0782453

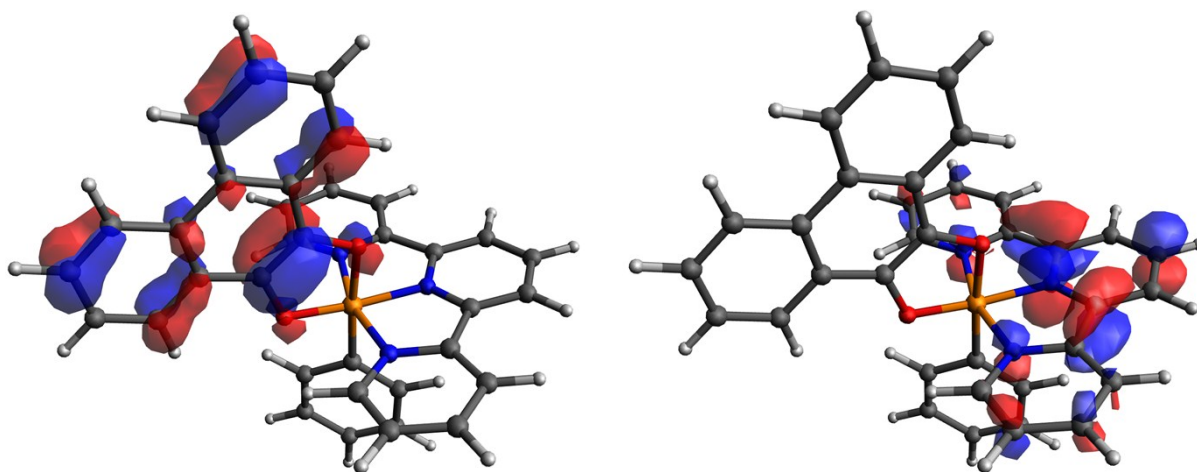


Figure S26. HOMO (left) and LUMO (right) of the cation of **5/6**.

5.2 Terpy-centered HDF mechanism with hydride delivery from Et₃SiH as the initial step

The following calculations are associated with the HDF mechanism in which the *para*-carbon of the central terpy ring acts as the hydride acceptor from Et₃SiH in the initial step (Figure S27):

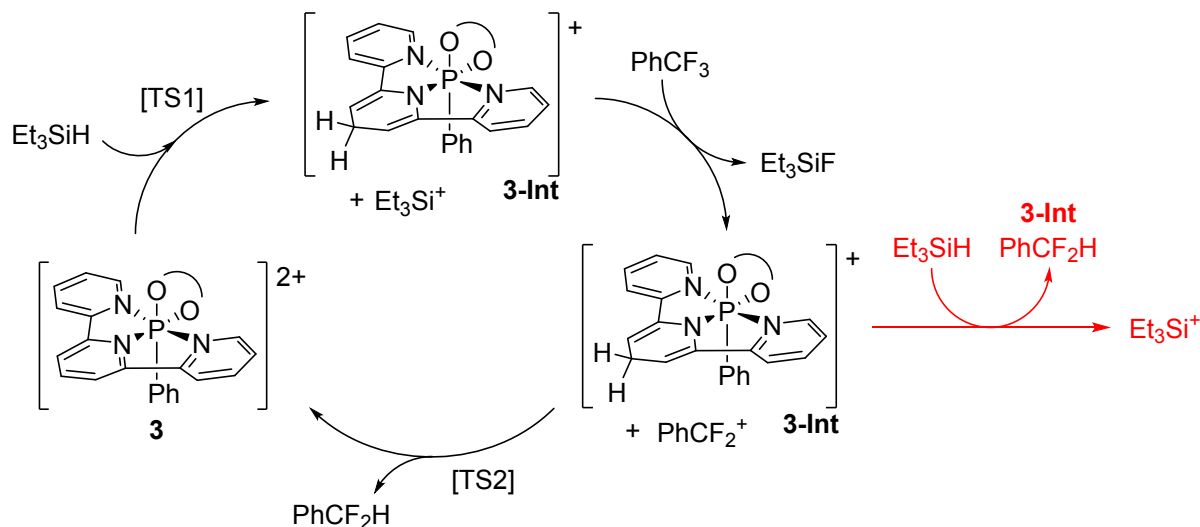


Figure S27. Proposed mechanism for the HDF of PhCF₃ to PhCF₂H via hydride delivery from Et₃SiH to the terpy ligand.

All computations were performed using the Gaussian 09 program.^[2] Geometry optimizations were performed at the M06-2X/Def2-SVP level of theory. Frequency calculations at the same level of theory were performed to identify the number of imaginary frequencies (zero for local minimum and one for transition states) and provide the thermal corrections of Gibbs free energy, which were added to the calculated single-point energies to obtain the Gibbs free energies in solution.

Table S3. Energies of Intermediates and Transition States

Compound	Single-Point Energy (Hartree)	Thermal Correction of Gibbs Free Energy (Hartree)
3	-3532.612074	0.318552
PhCF ₃	-568.659829	0.073458
Et ₃ SiH	-527.360743	0.168261
3-Int	-3533.525715	0.330376
PhCF ₂ ⁺	-468.598793	0.071752
Et ₃ Si ⁺	-526.486764	0.157253
PhCF ₂ H	-469.505961	0.083312
Et ₃ SiF	-626.568604	0.161964
[TS1]	-4059.969487	0.508044

 $[\text{Et}_3\text{Si} \cdots \text{H}]^{2+}$		
<p style="text-align: center;">[TS2]</p> $[\text{PhCF}_2 \cdots \text{H}]^{2+}$	-4002.073320	0.419650

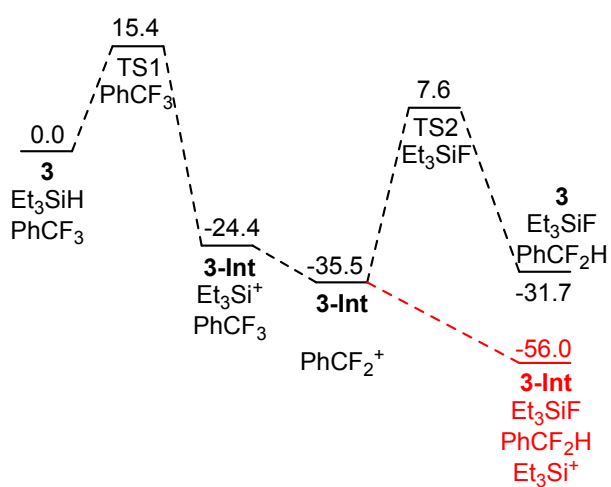


Figure S28. Calculated energies (kcal/mol) for the terpy-centered HDF mechanism of PhCF_3 to PhCF_2H

5.3 Phosphorus-centered HDF mechanism with hydride delivery from Et₃SiH as the initial step

The following calculations are associated with the HDF mechanism in which one of the pyridine rings initially dissociates, followed by the phosphorus-center acting as the hydride acceptor from Et₃SiH (Figure S29):

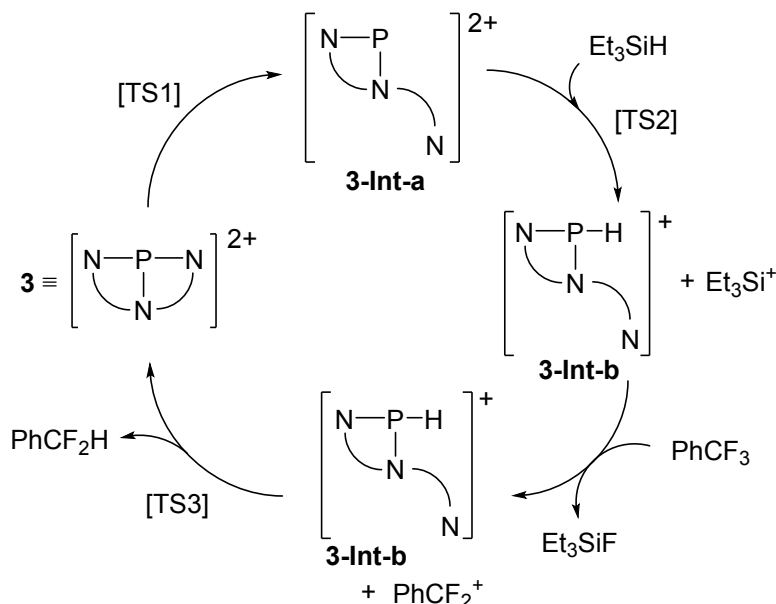
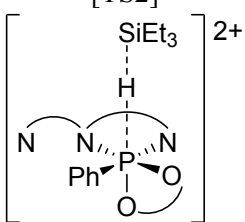
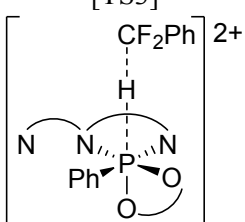


Figure S29. Proposed mechanism for the HDF of PhCF₃ to PhCF₂H *via* dissociation of terpy followed by hydride delivery from Et₃SiH to the phosphorus center.

All computations were performed using the Gaussian 09 program.^[2] Geometry optimizations were performed at the M06-2X/Def2-SVP level of theory. Frequency calculations at the same level of theory were performed to identify the number of imaginary frequencies (zero for local minimum and one for transition states) and provide the thermal corrections of Gibbs free energy, which were added to the calculated single-point energies to obtain the Gibbs free energies in solution.

Table S4. Energies of Intermediates and Transition States

Compound	Single-Point Energy (Hartree)	Thermal Correction of Gibbs Free Energy (Hartree)
3	-3532.612074	0.318552
PhCF ₃	-568.659829	0.073458
Et ₃ SiH	-527.360743	0.168261
3-Int-a	-3532.566633	0.316230
3-Int-b	-3533.495817	0.326692
PhCF ₂ ⁺	-468.598793	0.071752

Et ₃ Si ⁺	-526.486764	0.157253
PhCF ₂ H	-469.505961	0.083312
Et ₃ SiF	-626.568604	0.161964
[TS1]	-3532.564220	0.317288
[TS2] 	-4059.936065	0.509906
[TS3] 	-4002.033434	0.419903

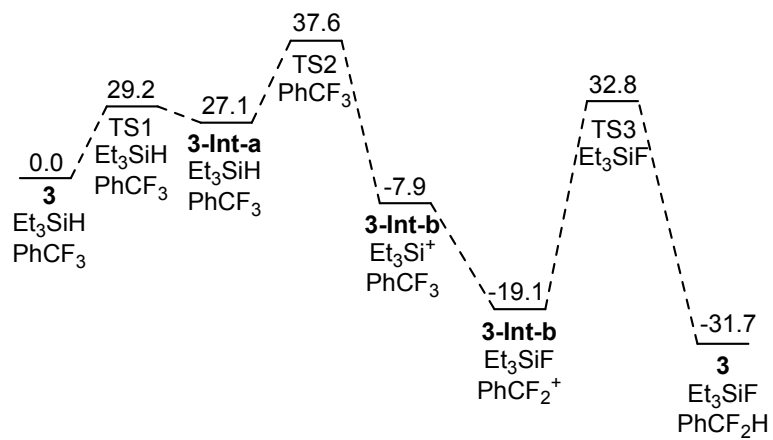


Figure S30. Calculated energies (kcal/mol) for the phosphorus-centered HDF mechanism of PhCF₃ to PhCF₂H

5.4 Terpy-centered HDF mechanism with fluoride delivery from PhCF₃ as the initial step

The following calculations are associated with the HDF mechanism in which the *para*-carbon of the central terpy ring acts as the fluoride acceptor from PhCF₃ in the initial step (Figure S31):

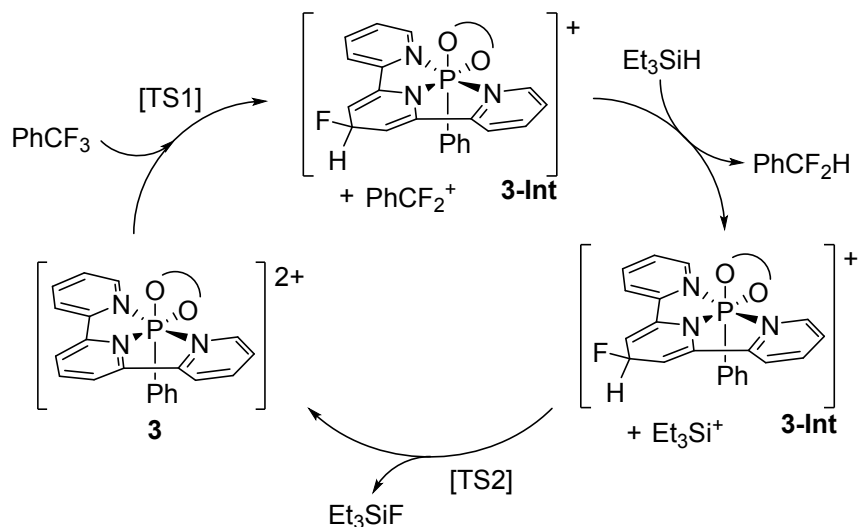


Figure S31. Proposed mechanism for the HDF of PhCF₃ to PhCF₂H via fluoride delivery from PhCF₃ to the terpy ligand.

All computations were performed using the Gaussian 09 program.^[2] Geometry optimizations were performed at the M06-2X/Def2-SVP level of theory. Frequency calculations at the same level of theory were performed to identify the number of imaginary frequencies (zero for local minimum and one for transition states) and provide the thermal corrections of Gibbs free energy, which were added to the calculated single-point energies to obtain the Gibbs free energies in solution.

Table S5. Energies of Intermediates and Transition States

Compound	Single-Point Energy (Hartree)	Thermal Correction of Gibbs Free Energy (Hartree)
3	-3532.612074	0.318552
PhCF ₃	-568.659829	0.073458
Et ₃ SiH	-527.360743	0.168261
3-Int	-3632.657271	0.319039
PhCF ₂ ⁺	-468.598793	0.071752
Et ₃ Si ⁺	-526.486764	0.157253
PhCF ₂ H	-469.505961	0.083312
Et ₃ SiF	-626.568604	0.161964
[TS1]	-4101.215082	0.410327

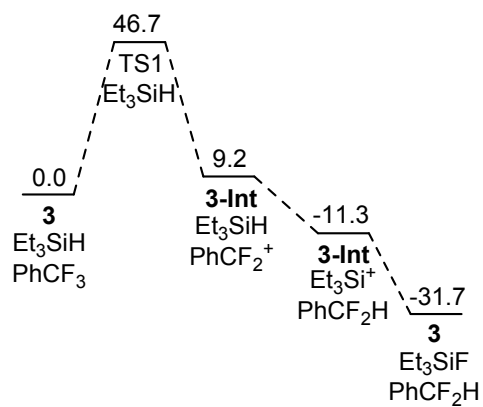
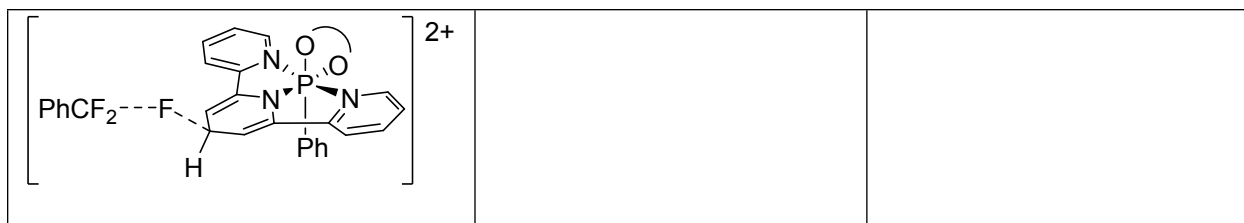


Figure S32. Calculated energies (kcal/mol) for the terpy-centered HDF mechanism of PhCF₃ to PhCF₂H

5.5 Phosphorus-centered HDF mechanism with fluoride delivery from PhCF₃ as the initial step

The following calculations are associated with the HDF mechanism in which one of the pyridine rings initially dissociates, followed by the phosphorus-center acting as the fluoride acceptor from PhCF₃ (Figure S33):

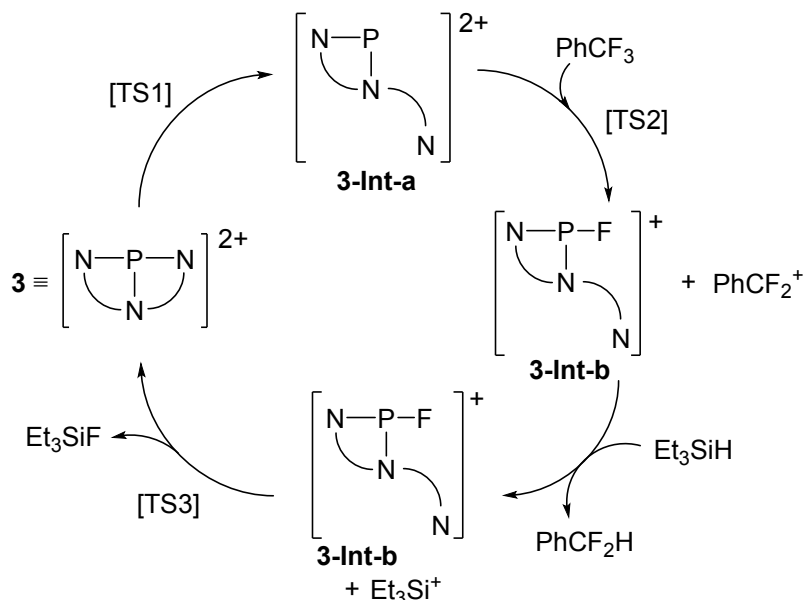
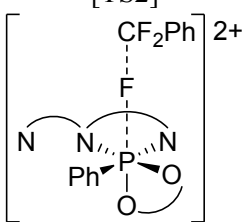


Figure S33. Proposed mechanism for the HDF of PhCF₃ to PhCF₂H via dissociation of terpy followed by fluoride delivery from PhCF₃ to the phosphorus center.

All computations were performed using the Gaussian 09 program.^[2] Geometry optimizations were performed at the M06-2X/Def2-SVP level of theory. Frequency calculations at the same level of theory were performed to identify the number of imaginary frequencies (zero for local minimum and one for transition states) and provide the thermal corrections of Gibbs free energy, which were added to the calculated single-point energies to obtain the Gibbs free energies in solution.

Table S6. Energies of Intermediates and Transition States

Compound	Single-Point Energy (Hartree)	Thermal Correction of Gibbs Free Energy (Hartree)
3	-3532.612074	0.318552
PhCF ₃	-568.659829	0.073458
Et ₃ SiH	-527.360743	0.168261
3-Int-a	-3532.566633	0.316230
3-Int-b	-3632.670856	0.319953
PhCF ₂ ⁺	-468.598793	0.071752

Et ₃ Si ⁺	-526.486764	0.157253
PhCF ₂ H	-469.505961	0.083312
Et ₃ SiF	-626.568604	0.161964
[TS1]	-3532.564220	0.317288
[TS2] 	-4101.220580	0.411624

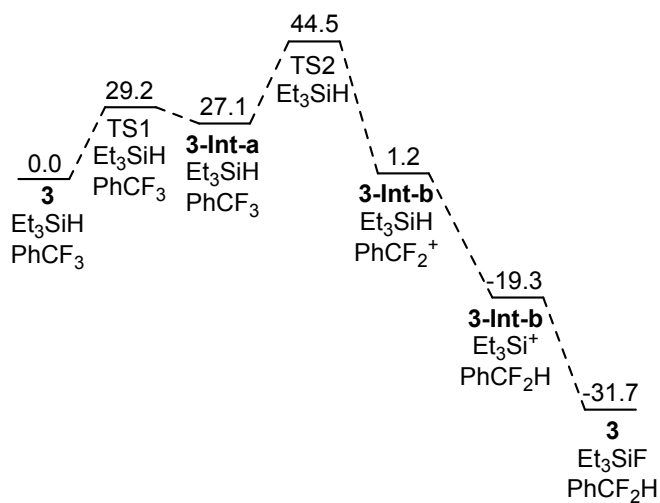


Figure S34. Calculated energies (kcal/mol) for the phosphorus-centered HDF mechanism of PhCF₃ to PhCF₂H

6. X-ray Crystallography

X-ray Data Collection and Reduction. Crystals were coated in Paratone-N oil in an N₂ filled glovebox, mounted on a MiTegen Micromount, and placed under a N₂ stream, thus maintaining a dry, O₂-free environment for each crystal. The data were collected on a Bruker Apex II diffractometer using a graphite monochromator with Mo K α radiation ($\lambda = 0.71073$ Å). The data were collected at 150(2) K for all crystals. The frames were integrated with the Bruker SAINT software package using a narrow-frame algorithm. The data were corrected for absorption effects using the empirical multi-scan method (SADABS).

Structure Solution and Refinement. The structures were solved by direct methods using XS and subjected to full-matrix least-squares refinement on F² using XL as implemented in the SHELXTL suite of programs. All non-hydrogen atoms were refined with anisotropically thermal parameters. Carbon-bound hydrogen atoms were placed in geometrically calculated positions and refined using an appropriate riding model and coupled isotropic thermal parameters.

Table S7. Summary of crystallographic data for **4** and **6**

	4	6
empirical formula	C ₂₉ H ₁₆ Cl ₄ F ₆ N ₃ O ₈ PS ₂	C ₄₃ H ₃₇ F ₆ N ₄ O ₉ PS ₂
formula weight	885.34	962.85
crystal system	Triclinic	Monoclinic
space group	<i>P</i> -1	<i>P</i> 2 ₁ / <i>n</i>
<i>a</i> (Å)	8.766(1)	10.6663(4)
<i>b</i> (Å)	10.806(2)	25.760(1)
<i>c</i> (Å)	19.768(3)	16.1421(7)
α (°)	95.710(8)	
β (°)	99.202(8)	100.574(2)
γ (°)	112.242(8)	
vol (Å ³)	1684.4(4)	4359.9(3)
<i>Z</i>	2	4
ρ (calcd) (Mg·m ⁻³)	1.746	1.467
μ (mm ⁻¹)	0.612	0.245
<i>F</i> (000)	888	1984
<i>T</i> (K)	150(2)	150(2)
reflections collected	22897	75513
unique reflections	5927	9611
R _{int}	0.0345	0.1187
R1 indices [<i>I</i> >2 σ (<i>I</i>)]	0.0377	0.0571
wR2 indices (all data)	0.1306	0.1927

7. References

- [1] S. C. Chitnis, F. Krischer, D. W. Stephan, *Chem. Eur. J.*, 2018, **24**, 6543-6546.
- [2] Gaussian 09, Revision E.01, M. J. Frisch, G. W. Trucks, H. B. Schlegel, G. E. Scuseria, M. A. Robb, J. R. Cheeseman, G. Scalmani, V. Barone, B. Mennucci, G. A. Petersson, H. Nakatsuji, M. Caricato, X. Li, H. P. Hratchian, A. F. Izmaylov, J. Bloino, G. Zheng, J. L. Sonnenberg, M. Hada, M. Ehara, K. Toyota, R. Fukuda, J. Hasegawa, M. Ishida, T. Nakajima, Y. Honda, O. Kitao, H. Nakai, T. Vreven, J. A. Montgomery Jr., J. E. Peralta, F. Ogliaro, M. J. Bearpark, J. Heyd, E. N. Brothers, K. N. Kudin, V. N. Staroverov, R. Kobayashi, J. Normand, K. Raghavachari, A. P. Rendell, J. C. Burant, S. S. Iyengar, J. Tomasi, M. Cossi, N. Rega, N. J. Millam, M. Klene, J. E. Knox, J. B. Cross, V. Bakken, C. Adamo, J. Jaramillo, R. Gomperts, R. E. Stratmann, O. Yazyev, A. J. Austin, R. Cammi, C. Pomelli, J. W. Ochterski, R. L. Martin, K. Morokuma, V. G. Zakrzewski, G. A. Voth, P. Salvador, J. J. Dannenberg, S. Dapprich, A. D. Daniels, Ö. Farkas, J. B. Foresman, J. V. Ortiz, J. Cioslowski, D. J. Fox, Gaussian, Inc., Wallingford, CT, USA, 2009.
- [3] NBO 6.0. E. D. Glendening, J. K. Badenhoop, A. E. Reed, J. E. Carpenter, J. A. Bohmann, C. M. Morales, C. R. Landis, and F. Weinhold (Theoretical Chemistry Institute, University of Wisconsin, Madison, WI, 2013); <http://nbo6.chem.wisc.edu/>